Water transport properties of virtual fractal porous media: implications for the unsaturated transport properties of cement-based materials

Stéphane Poyet

Version of Record: https://www.sciencedirect.com/science/article/pii/S0008884621002623
Manuscript_8715a2991c73ba96e4aafd05fa99d53e

Water transport properties of virtual fractal porous media: implications for the unsaturated transport properties of cement-based materials

Stéphane POYET *

* Université Paris-Saclay, CEA, Service d'Etude du Comportement des Radionucléides, F-91191, Gif-sur-Yvette, France

Contact

- Postal address: CEA Saclay, DES/ISAS/DPC/SECR/LECBA, B158 PC25, F-91191 Gif-sur-Yvette cedex, France
- Mail: stephane.poyet@cea.fr

Conflict of interest: none

Abstract

Cement-based materials are more and more recognized as fractal materials. From a practical point of view, fractality means that the pore size distribution can be described using fractal scaling law (i.e. power functions). Here, the simplest scaling law making use of a single fractal dimension was used to generate simple and virtual fractal porous media (based on bundles of parallel cylindrical pores). The capillary curve and permeability (relative and intrinsic) of the virtual porous media were then estimated through theoretical and numerical approaches. The results show that: (1) although bereft of any physical basis, van Genuchten equation bears some fractal information; (2) although highly flexible, van Genuchten equation fails to perfectly fit the capillary curves and can thus generate error in inverse analysis (for intrinsic permeability evaluation) and (3) there seems to be a relation between the intrinsic permeability and van Genuchten pressure parameter.

Keywords: Pore Size Distribution; Adsorption; Permeability; Fractal

1. Introduction

Concretes and cement-based materials are ubiquitous in construction because they are versatile and affordable. Even though they have been broadly used and studied for decades, they remain difficult to apprehend and describe because of their multiphasic, multiscale and porous nature. For instance the pore-structure itself spans over several orders of magnitude in dimension - from the angstrom (10^{-10} m) up to the micrometer (10^{-6} m) or more - and it is still not possible today to obtain a clear view of the whole pore-structure even with the use of different experimental techniques [1,2]. The main consequence is that some concrete macroscopic properties that are strongly dependent on the pore-structure (such as transport properties) remain difficult to assess and often have to be tested experimentally.

It has been however known for years that the pores – or at least a fraction of them – exhibit fractal properties [3–11]. This was proven for the smaller pores (C-S-H pores) using small-angle x-ray (SAXS) or neutron scattering (SANS) [3,4,6,12–18]; for the larger pores using image

analysis (optical and/or electronic microscopy) [6–8,19] and of course using mercury intrusion porosimetry (MIP) [20–26]. All these results are far from being consistent as there is a strong scatter in the resulting fractal dimension values (they all lie between 1.0 and 3.5). Moreover it has also been suggested recently, using MIP results, that the fractality of the pore-structure was scale-dependent; the fractal dimension would not be not unique and there would exist at least two dimension domains each having a different value of the fractal dimension [20–23,25,27]. The reader should keep in mind that MIP is a flawed technique that misallocates pore size and can generate damage [28–32] (and then misestimate fractal dimensions); all the evaluations obtained using MIP then only should be taken with great caution. However, the scale dependence of the MIP fractal dimensions is consistent with the scatter obtained with the other techniques. In the author's mind, the cementitious materials are more than likely to be multifractal materials although the corresponding scale domains and fractal dimensions remain uncertain.

Pore fractality is an important feature because it means that the pore structure is similar at different scales. From a mathematical point of view, this implies that the pore size distribution should follow a simple scaling law in the form of r^{-D} where r is the pore radius and D the fractal dimension (a constant) [33]. The pore-size distribution can then be described using with simple power functions. It is the objective of this article to take advantage of using these simple analytical equations that describe fractal pore-size distribution in order to generate virtual porous media to be used as model materials to study the water transport properties of unsaturated concretes.

2. Unsaturated transport properties

In low permeable unsaturated concretes, it was shown that water transport was mainly due to the permeation of liquid water [34]. It is then possible to describe unsaturated water transport using a single equation [35,36]:

$$\emptyset\left(\frac{\partial S}{\partial P}\right)\frac{\partial P}{\partial t} = div\left[\left(\frac{Kk_r}{\eta}\right)\underline{grad}(P)\right] \tag{1}$$

where ∅ is the porosity; S the saturation index; P pressure of liquid water in the pores (Pa); K intrinsic permeability (m²); k_r relative permeability to water and η water viscosity (Pa s).

It is common practice to use the equation proposed by van Genuchten [37] to fit the capillary curve (relationship between pressure P and saturation S):

$$\begin{cases} S(P) = \left[1 + \left(\frac{P}{P_0}\right)^{\frac{1}{1-m}}\right]^{-m} \\ P(S) = P_0\left(S^{-\frac{1}{m}} - 1\right)^{1-m} \end{cases} \tag{2}$$

where m and P_0 are two positive constant, P_0 is equivalent to a pressure (in Pa). The left-hand term of equation (1) then writes:

$$\emptyset\left(\frac{\partial S}{\partial P}\right) = -\frac{m\phi}{(m-1)P_0}\left(\frac{P}{P_0}\right)^{\frac{m}{1-m}}\left[1 + \left(\frac{P}{P_0}\right)^{\frac{1}{1-m}}\right]^{-1-m} \tag{3}$$

The relative permeability k_r is almost never characterized through experiments; rather it is commonly evaluated using the model proposed by Mualem [38] that uses the capillary curve as input data:

$$k_r = \sqrt{S}\left[\frac{\int_0^S \frac{du}{P(u)}}{\int_0^1 \frac{du}{P(u)}}\right]^2 \tag{4}$$

When van Genuchten equation [37] is used together with the model of Mualem [38], the well-known following simple analytical expression aka known as Mualem-van Genuchten (MVG) is obtained:

$$\begin{cases} k_r(S) = \sqrt{S}\left[1-\left(1-S^{\frac{1}{m}}\right)^{m}\right]^2 \\ k_r(P) = \left[1+\left(\frac{P}{P_0}\right)^{\frac{1}{1-m}}\right]^{-\frac{m}{2}}\left(1-\left(\frac{P}{P_0}\right)^{\frac{1}{1-m}}\left[1+\left(\frac{P}{P_0}\right)^{\frac{1}{1-m}}\right]^{-m}\right)^2 \end{cases} \quad (5)$$

Finally, it must be recalled that the value of the intrinsic permeability K is preferably assessed through inverse analysis as those measured using water or gas are known to overestimate flowrates [39].

3. Definition of a fractal porous medium (FPM)

3.1. Pore-size distribution, porosity

Here, the cementitious materials were considered as ordinary fractal materials, i.e. with a unique fractal dimension. This choice clearly goes against what is commonly observed (i.e. different fractal dimensions over different size ranges). This choice was made to favor the simplicity of the approach in order to test and illustrate ideas, but this was done to the detriment of representativeness… Let us consider a relative elementary volume (REV) of a virtual fractal porous material in which the pores are constituted of straight, independent and parallel open-ended cylinders of radius between R_m and R_M (with $R_M \gg R_m$). The REV is a cube of dimension L_0 in which the cumulated number of pores follows a fractal scaling [33,40–42]:

$$\forall r \in [R_m; R_M] \;\; N(\rho \geq r) = \left(\frac{r}{R_M}\right)^{-D} \quad (6)$$

where N is the cumulated number of pores of radius greater than r and D the fractal dimension (with $1 < D < 2$).

It is noticeable that, by definition, there is only one pore of radius R_M. Increasing the value of the fractal dimension obviously increases the total number of pores but also the relative contribution of the smallest pores (Figure 1).

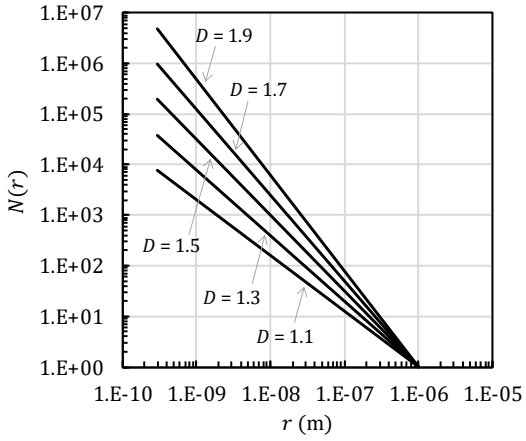

Figure 1: number of pores according to the fractal scaling ($R_m = 3 \times 10^{-10} m$ and $R_M = 1 \times 10^{-6}$ m)

The number of pores of radius r is easily obtained by differentiation of eq. (1):

$$n(r) = |dN| = DR_M^D r^{-D-1} dr \tag{7}$$

The total porosity ∅ of such a fractal porous medium is then:

$$\emptyset = \frac{1}{L_0^3}\int_{R_m}^{R_M}(\pi r^2 L_0)n(r) = \frac{\pi D R_M^D}{L_0^2}\int_{R_m}^{R_M} r^{2-D-1}dr = \frac{\pi D R_M^D}{(2-D)L_0^2}(R_M^{2-D} - R_m^{2-D}) \tag{8}$$

Expectedly, the value of the porosity depends on the pore-size interval $[R_m; R_M]$, fractal dimension D and also on the dimension of the REV L_0. The evaluation of the latter is not straightforward; in other words there is no evident exact method to evaluate L_0. Alternatively, an estimate can be obtained by considering that the porosity value ($\emptyset_0$) is known (it usually lies between 30 and 40% for hardened cement pastes), the REV dimension L_0 of a fractal hcp can then be estimated following:

$$\emptyset_0 = \frac{\pi D R_M^D}{(2-D)L_0^2}(R_M^{2-D} - R_m^{2-D}) \;\Rightarrow\; L_0 = \sqrt{\frac{\pi D R_M^D}{(2-D)\emptyset_0}(R_M^{2-D} - R_m^{2-D})} \tag{9}$$

Using $\emptyset_0 = 35\%$; $R_\mathrm{m} = 3 \times 10^{-10}$ m; $R_\mathrm{M} = 1 \times 10^{-6}$ m and $D = 1.5$ as input data, equation (4) yields $L_0 \approx 5 \times R_\mathrm{M}$ and then $L_0 \propto R_\mathrm{M}$.

3.2. Water retention

The water retention curve of the FPM was evaluated using a simple approach that considers that water is retained due to (*i*) physical adsorption of water molecules on the pore walls and (*ii*) capillary condensation [43–46] (more details in [47]). Adsorption was assumed to result in a unique water layer (monolayer), the thickness of which (t_w) was described using Langmuir's model [48]:

$$t_w(h) = \frac{k t_m h}{1+kh} \tag{10}$$

where h is the relative humidity (without unit); k Langmuir's equilibrium constant (without unit) and t_m the thickness of the complete monolayer (m). The value of these two parameters was set to $k = 50$ and $t_m = 3 \times 10^{-10}$ m (3 Å) following Morgan & Warren [49], Harkins & Jura [50], Hagymassy [51] and Yamanaka [52]. The pore saturation induced by adsorption is then:

$$S_a(h) = \frac{1}{\emptyset L_0^3}\int_{R_m}^{R_M}(2\pi r L_0)t_w(h)n(r) = 2t_w(h)\left(\frac{2-D}{1-D}\right)\left(\frac{R_M^{1-D} - R_m^{1-D}}{R_M^{2-D} - R_m^{2-D}}\right) \tag{11}$$

Capillary condensation was described using the well-known Kelvin equation that determines the maximal value of the pores radius r_K in which condensation occurs:

$$r_K(h) = -\frac{2M\sigma}{\rho R T ln(h)} \tag{12}$$

where M is the water molar mass (18×10^{-3} kg/mol); σ surface tension (0.072 N/m); ρ water density (998.3 kg/m^3 at 20°C); R ideal gas constant (8.3145 J/mol/K); T absolute temperature (273.15 K) and h relative humidity (without unit).

The reader must keep in mind that the presence of the adsorbed film reduces the apparent radius of the pores and thus condensation occurs in pores of radius lower than $(r_K + t_w)$ instead of r_K. The pore saturation induced by capillary condensation is then:

$$\begin{aligned} S_c(h) &= \frac{1}{\emptyset L_0^3}\int_{R_m}^{r_K+t_w}(\pi r^2 L_0)n(r) - \frac{1}{\emptyset L_0^3}\int_{R_m}^{r_K+t_w}(2\pi r L_0)n(r)t_w(h) \\ &= \left[\frac{(r_K+t_w)^{2-D} - R_m^{2-D}}{R_M^{2-D} - R_m^{2-D}}\right] - 2t_w(h)\left(\frac{2-D}{1-D}\right)\left[\frac{(r_K+t_w)^{1-D} - R_m^{1-D}}{R_M^{2-D} - R_m^{2-D}}\right] \end{aligned} \tag{13}$$

Eventually, the saturation is the sum of the two contributions (adsorption and condensation):

$$S(h) = S_c(h) + S_a(h) = \left[\frac{(r_K+t_w)^{2-D} - R_m^{2-D}}{R_M^{2-D} - R_m^{2-D}}\right] + 2t_w(h)\left(\frac{2-D}{1-D}\right)\left[\frac{R_M^{1-D} - (r_K+t_w)^{1-D}}{R_M^{2-D} - R_m^{2-D}}\right] \quad (14)$$

The saturation proves to be a simple analytical function, with only two terms that depend on the pore-size interval $[R_m; R_M]$ and fractal dimension D. it is noteworthy that when $(r_K + t_w)(h) = R_M$ all the pores are filled with water and then $S = 1$. Otherwise, when $(r_K + t_w)(h) = R_m$ there is no condensed water but the saturation is not nil because of the presence of the adsorbed film on the pore walls and so $S = 2t_w(h)\left(\frac{2-D}{1-D}\right)\left(\frac{R_M^{1-D} - R_m^{1-D}}{R_M^{2-D} - R_m^{2-D}}\right) > 0$.

3.3. Intrinsic permeability

To compute the permeability of the FPM, one must start with Poiseuille law that gives the flow through a cylinder of radius r and length L_0:

$$q(r) = \frac{\pi r^4}{8\eta}\left(\frac{\Delta P}{L_0}\right) \quad (15)$$

where μ is the dynamic viscosity of water (1.0016×10^{-3} Pa s at 20 °C) and ΔP the pressure difference between the inlet and outlet of the cylinder.

The flow through all the pores of the fractal porous medium is then the sum of the contributions of all the pores:

$$Q_t(r) = \int_{R_m}^{R_M}\left[\frac{\pi r^4}{8\eta}\left(\frac{\Delta P}{L_0}\right)\right] n(r) = \frac{\pi}{8\eta}\left(\frac{\Delta P}{L_0}\right) D R_M^D \int_{R_m}^{R_M} r^{3-D} dr = \frac{\pi D R_M^D}{8\eta(4-D)}\left(\frac{\Delta P}{L_0}\right)(R_M^{4-D} - R_m^{4-D}) \quad (16)$$

One can easily calculate the apparent permeability K_e of the fractal porous medium considering that:

$$Q_t(r) = \frac{K_e}{\eta} L_0^2 \left(\frac{\Delta P}{L_0}\right) = \frac{\pi D R_M^D}{8\eta(4-D)}\left(\frac{\Delta P}{L_0}\right)(R_M^{4-D} - R_m^{4-D}) \;\Rightarrow\; K_e = \frac{\pi D R_M^D}{8(4-D)L_0^2}(R_M^{4-D} - R_m^{4-D}) \quad (17)$$

It is clear here that the pores were assumed to be straight (without tortuosity); this was done on purpose to make the model as simple as possible and also because pore-tortuosity is already accounted for in Mualem model [38] and there was no use of accounting for it twice. The reader should however be informed that it is possible to include tortuosity using a supplementary fractal scaling law for the pore length L_0 [53–58].

As for the porosity, the permeability of the FPM is a function of the pore-size interval $[R_m; R_M]$, fractal dimension D and also on the dimension of the REV L_0. Yet, remembering that $L_0 \propto R_M$ and that $R_M \gg R_m$ it becomes obvious that $K_e \propto R_M^2$. This result is not surprising as it appears similar to the model proposed by Katz & Thompson based on percolation theory [59,60]:

$$K_e = \frac{F}{226} d_c^2 \propto d_c^2 \quad (18)$$

where F is the formation factor ($0 < F < 1$) that accounts for pore structure conformation and tortuosity and d_c is the critical pore entry diameter that corresponds to the inflexion point in the intrusion curve obtained using MIP. In other words, d_c is the greatest pore diameter that allow entry to the porous network and it seems reasonable that $d_c \approx 2R_M$.

Also note that equation (17) can alternatively be rewritten to include porosity $\emptyset$ as suggested by Guarracino [61], this presents the major advantage to flush the cumbersome parameter L_0:

$$K_e = \frac{\emptyset}{8}\left(\frac{2-D}{4-D}\right)\left(\frac{R_M^{4-D} - R_m^{4-D}}{R_M^{2-D} - R_m^{2-D}}\right) \;\Rightarrow\; K_e \propto \emptyset R_M^2 \quad (19)$$

3.4. Relative permeability

Mualem's model [38] was used to evaluate the relative permeability k_r of the FPM (eq. 4). Even though the equations used here are quite simple, it was not possible to derive an analytical expression for the function $P(S)$; because of the two different exponents $(2-D)$ and $(1-D)$ in eq 14). Alternatively, k_r was evaluated using the trapezoidal rule of Riemann sums following the original proposition of Mualem [38,62]. The saturation interval [0;1] was discretized into $n = 10^4$ intervals forming a non-uniform grid with $u_0 = 0$ (dry state) and $u_n = 1$ (saturated state) and the numerator in eq. (4) then wrote:

$$\begin{cases} \int_0^S \frac{du}{P(u)} = \sum_{i=1}^{m} (u_i - u_{i-1}) \left(\frac{1}{P_i} + \frac{1}{P_{i-1}} \right) \\ with\ 1 \le m \le (n-1) \mid S = u_m \end{cases} \quad (20)$$

where u_i is the saturation value of the i^{th} interval of the non-uniform grid and P_i the corresponding value of the water pressure (MPa).

It is obvious that $P_n^{-1} = \infty$, so the denominator in eq. (20) cannot be evaluated numerically. To overcome this difficulty, the surface area of the last trapezoid was not accounted in the summation and the relative permeability was then calculated as follows:

$$k_r(S) = \sqrt{u_m} \left[\frac{\sum_{i=1}^{m} (u_i - u_{i-1}) \left(\frac{1}{P_i} + \frac{1}{P_{i-1}} \right)}{\sum_{i=1}^{n-1} (u_i - u_{i-1}) \left(\frac{1}{P_i} + \frac{1}{P_{i-1}} \right)} \right]^2 \quad with\ 1 \le m \le (n-1) \quad (21)$$

The quality of the numerical approximation was tested by comparing the relative permeability curves evaluated using eq. (21) to those obtained using usual MVG analytical equation (eq. 5). The results are presented in Figure 2. The numerical approximation scheme did provide an almost perfect match with the analytical equation despite the fact that one trapezoid surface area was neglected.

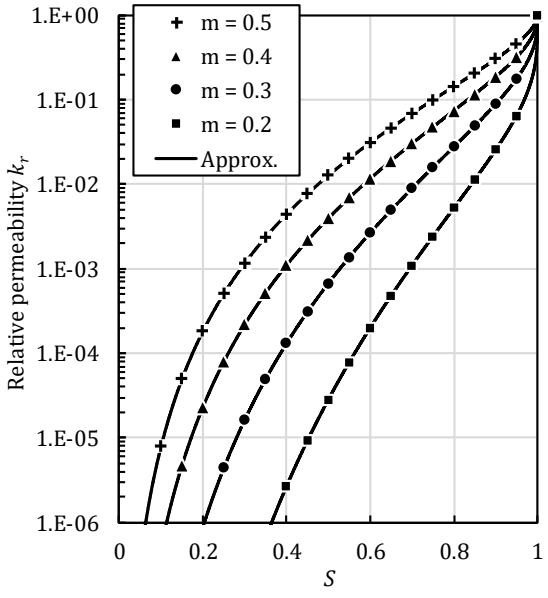

Figure 2: comparison between numerical approximation (eq. 21) and MVG analytical equation (eq. 5)

4. Results

4.1. Water retention

Figure 3 presents some water retention curves that were obtained for the FPM using eq. (14) and the following data:

- the minimal pore radius R_m was assumed to be constant and equal to the monolayer thickness to allow the edification of a monolayer in the smallest pores ($R_m = t_m = 3 \times 10^{-10}$ m);
- the maximal pore radius R_M was varied between 10 nm and 1 µm (1×10^{-8} m $\leq R_M \leq 1 \times 10^{-6}$ m);
- the fractal dimension was varied between 1.1 and 1.9 ($1.1 < D < 1.9$).

The reader can observe that the water retention curves of the virtual FPM are of type IV [63] and that they are quite similar to the desorption isotherms of common cement-based materials [64–68]. Figure 3(a) underscores the influence of the fractal dimension D and Figure 3(b) the influence of the maximal pore radius R_M. Increasing the fractal dimension D mainly results in increasing the saturation value at low RH (*i.e.* the monolayer) because it controls the pore number distribution and the thus the relative contribution of the smaller pores (Figure 1). The maximal pore radius R_M exhibits two distinct effects: firstly decreasing the value of R_M increases the length of the plateau at high RH through Kelvin equation (7) and secondly changing the value of R_M also impacts the pore number distribution (and then the contribution of the smaller pores) through equation (1).

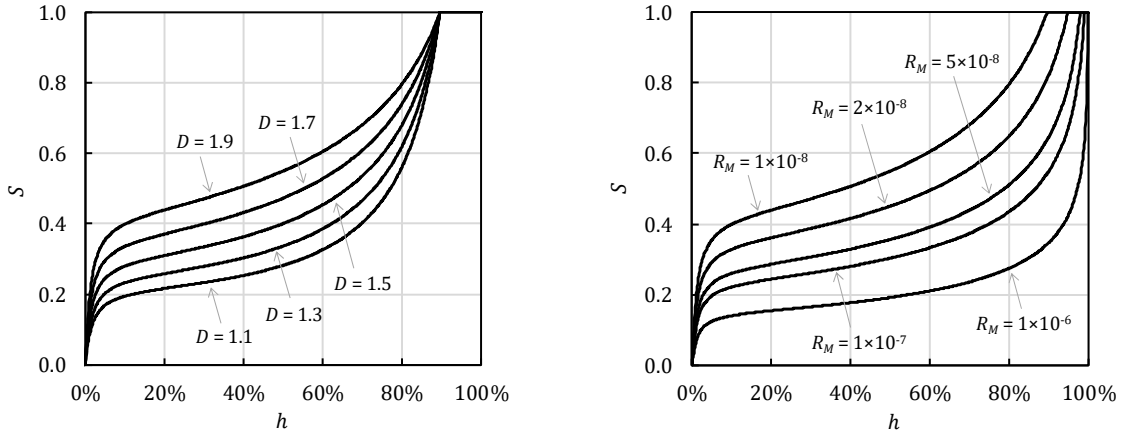

(a) influence of D ($R_M = 5 \times 10^{-8}$ m) (b) influence of R_M ($D = 1.9$)

Figure 3: influence of R_M and D on the water retention curve

All the water retention curves were fitted using van Genuchten equation (18) using a classical least-square minimization process. It must be mentioned here that, despite its deemed great adaptability, van Genuchten equation (2) did not provide a good fit for all the water retention curves. This was particularly obvious with small values of R_M that generated large plateaus at high RH that could not be described using van Genuchten (Figure 4), because van Genuchten implicitly assumed that the pore size distribution is unbounded and that $S = 1$ only when $P \to \infty$. Actually, this observation proved to be valid for all the tested cases (Figure 12), this was already observed and discussed elsewhere [62].

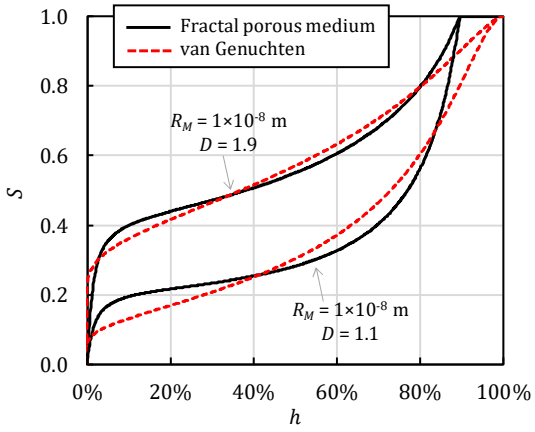

Figure 4: examples of poor fits obtained using van Genuchten equation

The values of the two parameters P_0 and m were found to depend on both fractal dimension D and maximal pore radius R_M (Figure 5) but further examination of these results unexpectedly showed that the exponent m was more or less a function of the fractal dimension D alone and that the pressure P_0 was a function of the maximal pore radius R_M alone (Figure 6). Roughly speaking, the m-exponent is a measure of the fractal dimension ($m \propto -D$) whereas the bubbling pressure P_0 is a measure of the bigger pores dimension ($P_0 \propto R_M^{-1}$). This result is surprising because van Genuchten equation was proposed to provide an analytical solution to Mualem's model without any physical basis. Note that the similarities between van Genuchten model and fractal approaches were already noted and discussed by Hunt [69].

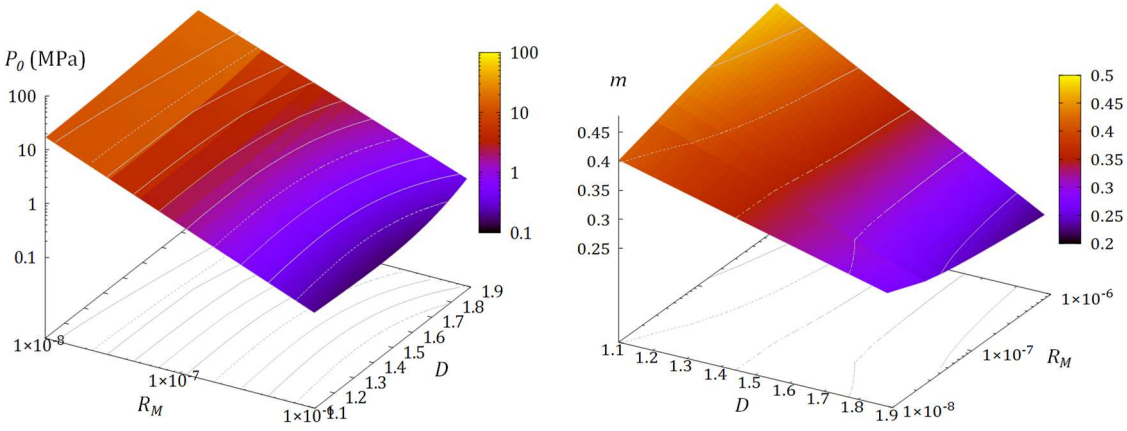

(a) P_0 versus R_M & D (b) m versus D & R_M

Figure 5: influence of R_M and D on van Genuchten parameters (m, P_0)

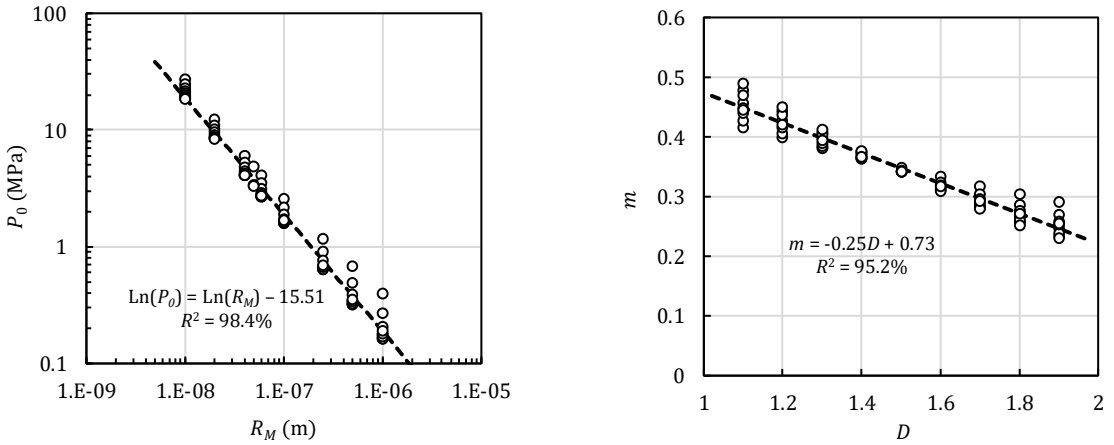

(a) P_0 versus R_M ($1.1 \leq D \leq 1.9$) (b) m versus D (1×10^{-8} m $\leq R_M \leq 1 \times 10^{-6}$ m)

Figure 6: compilation of all the results from Figure 5 showing that $m \propto -D$ and $P_0 \propto R_M^{-1}$

To go further in studying the "fractal nature" of van Genuchten equation, Figure 7 depicts the influence of the two parameters m and P_0 on the water retention curve. It is plain to see that m mainly controls the saturation at low RH (Figure 7-a) as is the case with the fractal dimension D (Figure 3-a). The same holds true for the pressure P_0 (Figure 7-b) and the maximal pore radius R_M (Figure 3-b) that generate a plateau at high RH and also impact the saturation at low RH.

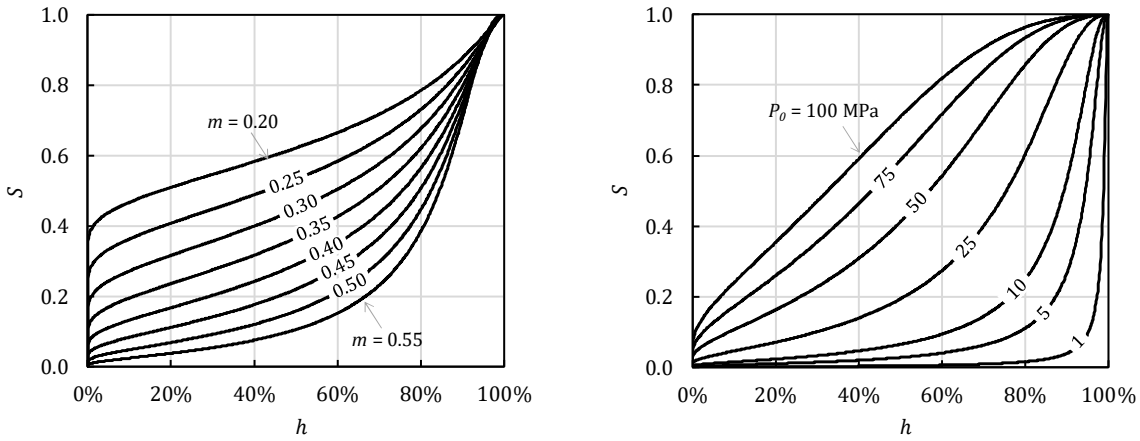

(a) Influence of m ($0.15 < m < 0.55$) (b) Influence of P_0 ($1 < P_0 < 100$ MPa)

Figure 7: influence of P_0 and m on van Genuchten water retention curves

4.2. Intrinsic permeability

Figure 8 shows that the intrinsic permeability K_e of the FPM (eq. 17) was ranging between 10^{-18} m^2 and 10^{-15} m^2. Despite the fact that no tortuosity was introduced in the description, the latter results did present the same order of magnitude as the permeability values measured using gas [70–72]. The reader should keep in mind that the values obtained using water are much lower than using gas [70,73]. This may be due to the change in microstructure induced by the drying (necessary for the gas permeability tests) [74,75] and also to electrical interactions between the solvent (water is a polar molecule) and the pore walls that limit the mobility of water and then decreases permeability [76–80]. As for tortuosity, water-substrate interactions were not accounted for here; so gas permeability results were the most appropriate to compare with.

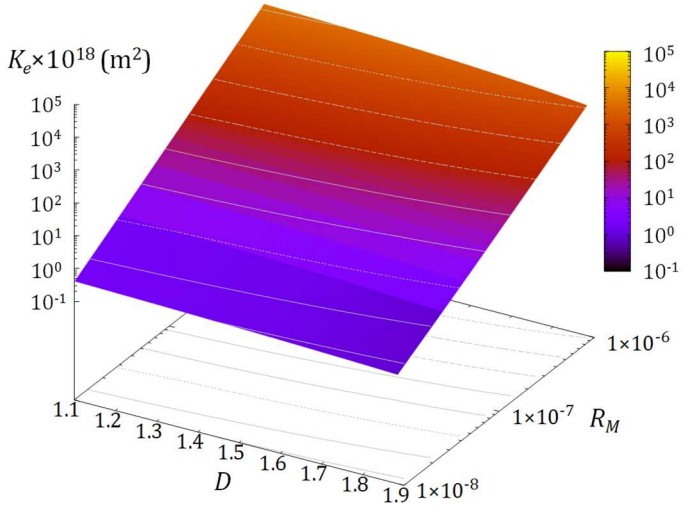

Figure 8: influence of D and R_M on the intrinsic permeability K_e of the fractal porous medium

Examining Figure 8, it is plain to see that the intrinsic permeability K_e of the FPM is mostly influenced by the maximal pore radius R_M. Remembering that the pressure P_0 was a measure of R_M then a relation between K_e and R_M should exist: $K_e \propto P_0^{-2}$. Note that this was already noted and verified by Guarracino [61] for a large soil dataset.

In an attempt to check the existence of such a relation for cement-based materials, some permeability results obtained using inverse analysis were plotted in Figure 9 and some piece of corresponding information was reported in Table 1. It is plain to notice that all the results were obtained by the same author: it was a deliberate choice (but this could called into question) not to include the results obtained by other researchers because it would have induced too much scatter as inverse analysis is known to be a highly sensitive method [36,62]. Also note that the results also include data obtained using the cup-method as it was shown to give similar results to inverse analysis [81]. The results include non-carbonated and carbonated concretes and pastes that yielded variations in P_0 and K of two and four orders of magnitude respectively.

All the points almost align along the curve $K(P_0) = AP_0^{-2}$ (with $A \approx 3.0 \times 10^{-19}$ m^2) but with some scatter that remained encouragingly less than one order of magnitude. It must be recalled that the method proposed by Katz and Thompson [59,60] that is commonly used to evaluate the intrinsic permeability based on MIP tests [82–84] is known to present large differences (up to two orders of magnitude for low-permeable materials) [85–88]. Of course, there are not enough data to judge the existence and quality of the proposed correlation and more results would be necessary and the readers are invited to test this correlation using their own results. Yet, such a correlation would be very useful because it would allow the intrinsic permeability to be estimated using the water retention curve (similarly to the relative permeability through Mualem model) and then reduce the number of tests needed to characterize the water transport properties. Finally, the reader should keep in mind that such a correlation would be fluid dependent.

Table 1: permeability results plotted in Figure 9

Reference	Materials	Composition/remarks	Method
Poyet et al. (2011) [36]	Concrete	Old concrete, highly porous and permeable Unknown composition	Inverse analysis
Drouet et al. (2015) [89]	Paste	4 different binders, w/c = 0.40	Inverse analysis
Auroy et al. (2015) [81]	Paste	Same pastes as Drouet et al. (2015) [89]	Inverse analysis + cup-method
Poyet et al. (2019) [90]	Concrete	Low permeable OPC concrete (w/c = 0.42)	Inverse analysis

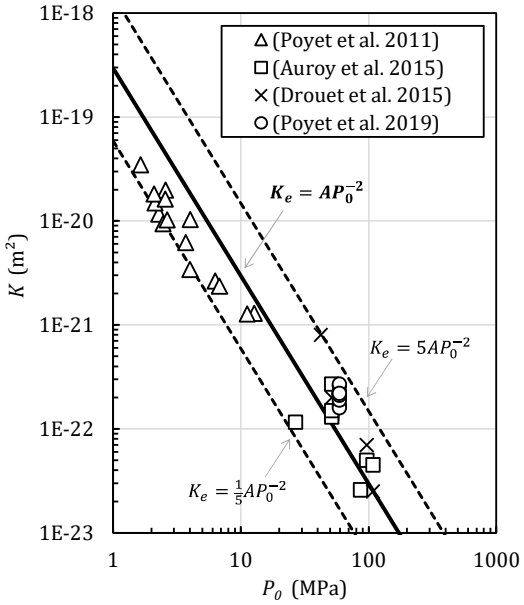

Figure 9: intrinsic permeability K versus P_0, from [36], [89], [81] *and* [90]

4.3. Relative permeability

Figure 10 compares the relative permeability of some fractal porous media obtained using Mualem's model (eq. 4) to those obtained using van Genuchten equation (eq. 5). For the sake of clarity, only three values of D (1.1, 1.5 and 1.9) are displayed and for each five values of R_M (10^{-8}, 2×10^{-8}, 5×10^{-8}, 10^{-7} and 10^{-6} m). It was clear that the relative permeability k_r of the FPM (Figure 10-a) was a function of D and R_M, although the fractal dimension appeared to be the most influential parameter. It should be mentioned that the unusual change of slope occurring in some curves below 0.4 in saturation (D = 1.9) was due to the strong knee that was obtained for small R_M values (see Figure 3 and Figure 4).

The use of van Genuchten equation (Figure 10-b) did not appear to be satisfactory as it clearly led to underestimate the k_r values (Figure 11). This underestimation was due to the limited fitting ability of van Genuchten equation that was not able to perfectly fit the water retention curves of all the FPM. This was already noted for small R_M values because of the plateau at high saturation (Figure 4) but this conclusion was found to be valid in all cases, even for high values of R_M. The isotherms obtained using van Genuchten all showed differences with those of the FPM (Figure 12) even though they could not be detected using the naked eye in most cases. The point was that these differences, even small, were responsible through Mualem's model, of the underestimation by one order of magnitude that was observed in Figure 11. This last point is important because it sheds light on the subject of the permeability of cement-based materials and more specifically on the fact the permeability values to be used in simulations (through inverse analysis) are smaller than those measured using water [39]. Part of these differences might be explained by vanGenuchten equation and its limited fitting ability because inverse analysis is known to be very dependent on the input data and the models that are used [62].

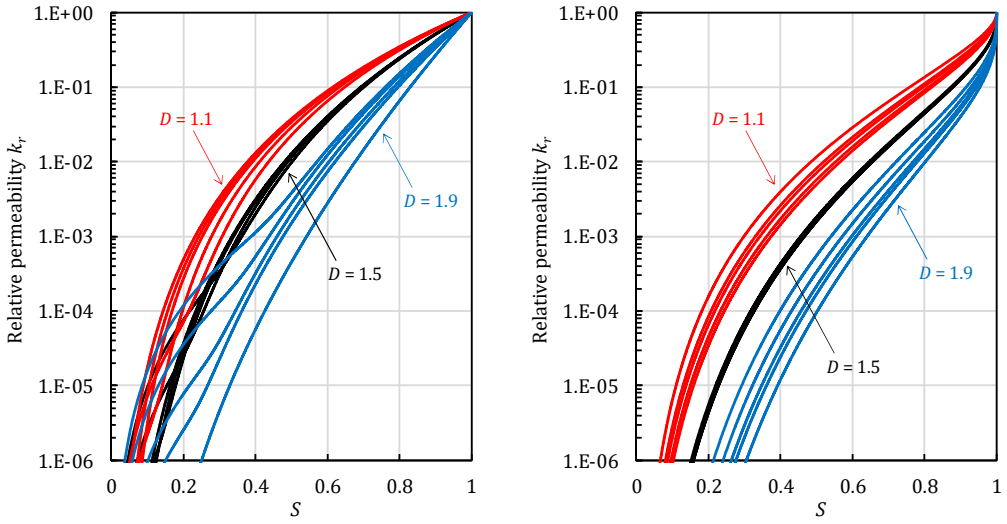

(a) numerical approximation (ref.) (b) MVG analytical equation

Figure 10: comparison between the relative permeability k_r curves obtained using either the numerical approximation (eq. 21) or the MVG analytical expression (eq. 5)

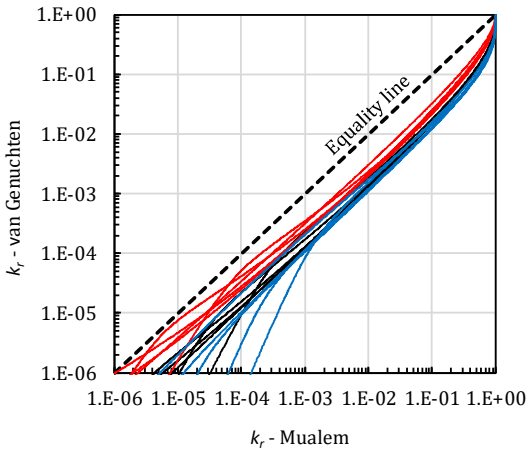

Figure 11: comparison between the k_r values obtained using the numerical approximation (eq. 21) or the MVG analytical equation (eq. 5)

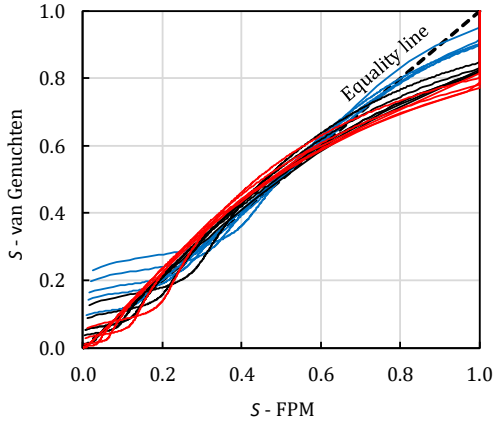

Figure 12: comparison of the capillary curves obtained of the virtual FPM (eq. 14) and fitted using van Genuchten equation (eq. 2)

5. Conclusion

The pore-structure of cement-based materials is more and more recognized as being fractal. The mathematical meaning of fractality is the existence of a simple analytical pore scaling law (in the form of a power function). Using this scaling law and considering a single fractal dimension, it was easy to generate virtual and simple fractal porous media that were then used to study some important water transport properties (intrinsic and relative permeability and water retention curve) and the associated Mualem model and van Genuchten equations. It must be recalled here that due to their simplicity (single fractal dimension) the virtual fractal porous media may not be representative of the real cement-based materials.

Firstly, van Genuchten equation was used to fit the capillary curves that were generated considering physical adsorption and capillary condensation. It appeared that, although bereft of any physical basis, van Genuchten equation may be considered as bearing some physical information because its two parameters were closely related to the fractal porous media properties: the exponent m was a measure of the fractal dimension (D) whereas the pressure P_0 was a measure of the maximal pore radius (R_M).

Secondly, the capillary curves were used to evaluate the relative permeability (making use of Mualem model). Although it is known to be flexible, van Genuchten equation did not provide perfect fits and the differences between the fitted capillary curves and those of the fractal porous media were sufficient to generate significant error: the relative permeability values were systematically underestimated up to one order of magnitude. This partly explains why the intrinsic permeability values obtained using inverse analysis are always lower than the measured ones. This also confirms the strong dependence of inverse analysis upon the models and data used.

Finally, the equations regarding permeability of the fractal porous media suggested that there should exist a relation between the intrinsic permeability and van Genuchten parameter P_0. Analysis of some results of the author tended to confirm the existence of such relationship even though the number of results are not sufficient to conclude. Such a relationship would prove extremely useful because it could help reducing the number of tests needed to describe water transport.

Acknowledgments

The free use of the mathematical code wxMaxima is greatfully acknowledged (https://wxmaxima-developers.github.io/wxmaxima/)

6. Bibliography

[1] J.J. Beaudouin, J. Marchand, Pore Structure (chapter 14), in: Handb. Anal. Tech. Concr., 2009: pp. 528–628. https://doi.org/10.1520/stp39427s.

[2] K. Scrivener, R. Snellings, B. Lothenbach, eds., A practical guide to microstructural analysis of cementitious materials, CRC Press, 2016.

[3] D.A. Winslow, The Fractal nature of the surface of cement paste, Cem. Concr. Res. 15 (1985) 817–824.

[4] A.J. Allen, R.C. Oberthur, D. Pearson, P. Schofield, C.R. Wilding, Development of the fine porosity and gel structure of hydrating cement systems, Philos. Mag. B. 56 (1987) 263–288.

[5] R. Blinc, G. Lahajnar, S. Žumer, NMR study of the time evolution of the fractal geometry of cement gels, Phys. Rev. B. 38 (1988) 2873–2875.

[6] V.M. Castaño, G. Martinez, J.L. Alemán, A. Jiménez, Fractal structure of the pore surface of hydrated portland cement pastes, J. Mater. Sci. Lett. 9 (1990) 1115–1116. https://doi.org/10.1007/BF00727895.

[7] D.A. Lange, H.M. Jennings, S.P. Shah, Image analysis techniques for characterization of pore structure of cement-based materials, Cem. Concr. Res. 24 (1994) 841–853. https://doi.org/10.1016/0008-8846(94)90004-3.
[8] S. Diamond, Aspects of concrete porosity revisited, Cem. Concr. Res. 29 (1999) 1181–1188. https://doi.org/10.1016/S0008-8846(99)00122-2.
[9] G.A. Niklasson, Adsorption on fractal structures: applications to cement materials, Cem. Concr. Res. 23 (1993) 1153–1158. https://doi.org/10.1016/0008-8846(93)90175-9.
[10] H.M. Jennings, Refinements to colloid model of C-S-H in cement : CM-II, Cem. Concr. Res. 38 (2008) 275–289. https://doi.org/10.1016/j.cemconres.2007.10.006.
[11] C. Porteneuve, J.P. Korb, D. Petit, H. Zanni, Structure-texture correlation in ultra-high-performance concrete: A nuclear magnetic resonance study, Cem. Concr. Res. 32 (2002) 97–101. https://doi.org/10.1016/S0008-8846(01)00635-4.
[12] M. Kriechbaum, G. Degovics, J. Tritthart, P. Laggner, Fractal structure of Portland cement paste during age hardening analyzed by small-angle x-ray scattering, Prog. Colloid Polym. Sci. 79 (1989) 101–105. https://doi.org/10.1007/bfb0116194.
[13] A. Heinemann, H. Hermann, K. Wetzig, F. Häussler, H. Baumbach, M. Kröning, Fractal microstructures in hydrating cement paste, J. Mater. Sci. Lett. 18 (1999) 1413–1416. https://doi.org/10.1023/A:1006671423783.
[14] A. Heinemann, H. Hermann, F. Häussler, SANS analysis of fractal microstructures in hydrating cement paste, Phys. B Condens. Matter. 276–278 (2000) 892–893. https://doi.org/10.1016/S0921-4526(99)01279-X.
[15] D. Winslow, J.M. Bukowski, J.F. Young, The fractal arrangement of hydrated cement paste, Cem. Concr. Res. 25 (1995) 147–156.
[16] T. Ficker, A. Len, P. Němec, Notes on hydrated cement fractals investigated by SANS, J. Phys. D. Appl. Phys. 40 (2007) 4055–4059. https://doi.org/10.1088/0022-3727/40/13/023.
[17] R.E. Beddoe, K. Lang, Effect of moisture on fractal dimension and specific surface of hardened cement paste by small-angle x-ray scattering, Cem. Concr. Resear. 24 (1994) 605–612.
[18] A.J. Allen, J.J. Thomas, Analysis of C-S-H gel and cement paste by small-angle neutron scattering, Cem. Concr. Res. 37 (2007) 319–324. https://doi.org/10.1016/j.cemconres.2006.09.002.
[19] J. Konkol, G. Prokopski, The use of fractal geometry for the assessment of the diversification of macro-pores in concrete, Image Anal. Stereol. 30 (2011) 89–100. https://doi.org/10.5566/ias.v30.p89-100.
[20] S. Jin, J. Zhang, S. Li, M. Fan, Basic study on fractal characteristic of pore structure in cement mortar, in: Y. Wang, P. Yi, S. An, H. Wang (Eds.), 9th Int. Conf. Chinese Transp. Prof., ASCE Pub., Harbin (China), 2009: pp. 2801–1807.
[21] X. Ji, S.Y.N. Chan, N. Feng, Fractal model for simulating the space-filling process of cement hydrates and fractal dimensions of pore structure of cement-based materials, Cem. Concr. Res. 27 (1997) 1691–1699.
[22] Q. Zeng, K. Li, T. Fen-Chong, P. Dangla, Surface fractal analysis of pore structure of high-volume fly-ash cement pastes, Appl. Surf. Sci. 257 (2010) 762–768. https://doi.org/10.1016/j.apsusc.2010.07.061.
[23] Q. Zeng, M. Luo, X. Pang, L. Li, K. Li, Surface fractal dimension: An indicator to characterize the microstructure of cement-based porous materials, Appl. Surf. Sci. 282 (2013) 302–307. https://doi.org/10.1016/j.apsusc.2013.05.123.
[24] X. Chen, J. Zhou, N. Ding, Fractal charcaterization of pore system evolution in cementitious materials, KSCE J. Civ. Eng. 19 (2015) 719–724.
[25] Y. Gao, K. Wu, J. Jiang, Examination and modeling of fractality for pore-solid structure in cement paste: Starting from the mercury intrusion porosimetry test, Constr. Build. Mater. 124 (2016) 237–243. https://doi.org/10.1016/j.conbuildmat.2016.07.107.
[26] S. Jin, J. Zhang, S. Han, Fractal analysis of relation between strength and pore structure of hardened mortar, Constr. Build. Mater. 135 (2017) 1–7. https://doi.org/10.1016/j.conbuildmat.2016.12.152.
[27] Y. Gao, K. Wu, Q. Yuan, Limited fractal behavior in cement paste upon mercury intrusion porosimetry test: Analysis and models, Constr. Build. Mater. 276 (2021) 122231. https://doi.org/10.1016/j.conbuildmat.2020.122231.
[28] D. Shi, D.N. Winslow, Contact angle and damage during mercury intrusion into cement paste, Cem. Concr. Res. 15 (1985) 645–654. https://doi.org/10.1017/CBO9781107415324.004.
[29] R.A. Olson, C.M. Neubauer, H.M. Jennings, Damage to the Pore Structure of Hardened Portland Cement Paste by Mercury Intrusion, J. Am. Ceram. Soc. 80 (1997) 2454–2458. https://doi.org/10.1111/j.1151-2916.1997.tb03144.x.

[30] S. Diamond, Mercury porosimetry. An inappropriate method for the measurement of pore size distributions in cement-based materials, Cem. Concr. Res. 30 (2000) 1517–1525. https://doi.org/10.1016/S0008-8846(00)00370-7.
[31] S. Chatterji, A discussion of the paper "mercury porosimetry - An inappropriate method for the measurement of pore size distributions in cement-based materials" by S. Diamond [1] (multiple letters), Cem. Concr. Res. 31 (2001) 1653–1654. https://doi.org/10.1016/S0008-8846(01)00616-0.
[32] J.P. Gorce, N.B. Milestone, Probing the microstructure and water phases in composite cement blends, Cem. Concr. Res. 37 (2007) 310–318. https://doi.org/10.1016/j.cemconres.2006.10.007.
[33] B.B. Mandelbrot, The Fractal Geometry of Nature (2nd Ed.), WH Freeman and Company, New York (USA), 1984.
[34] M. Mainguy, O. Coussy, V. Baroghel-Bouny, Role of air pressure in drying of weakly permeable materials, J. Eng. Mech. 127 (2001) 592–592.
[35] O. Coussy, Poromechanics, John Wiley & Sons, Ltd, Chichester (England), 2004.
[36] S. Poyet, S. Charles, N. Honoré, V. L'Hostis, Assessment of the unsaturated water transport properties of an old concrete: Determination of the pore-interaction factor, Cem. Concr. Res. 41 (2011) 1015–1023. https://doi.org/10.1016/j.cemconres.2011.06.002.
[37] M.T. van Genuchten, A Closed-form Equation for Predicting the Hydraulic Conductivity of Unsaturated Soils, Soil Sci. Soc. Am. J. 44 (1980) 892–898. https://doi.org/10.2136/sssaj1980.03615995004400050002x.
[38] Y. Mualem, A new model for predicting the hydraulic conductivity of unsaturated porous media, Water Resour. Res. 12 (1976) 513–522. https://doi.org/http://doi.wiley.com/10.1029/WR012i003p00513.
[39] V. Baroghel-Bouny, Water vapour sorption experiments on hardened cementitious materials. Part II: Essential tool for assessment of transport properties and for durability prediction, Cem. Concr. Res. 37 (2007) 438–454. https://doi.org/10.1016/j.cemconres.2006.11.017.
[40] S.W. Tyler, S.W. Wheatcraft, Fractal processes in soil water retention, Water Resour. Res. 26 (1990) 1047–1054.
[41] S.W. Tyler, S.W. Wheatcraft, Fractal Scaling of Soil Particle-Size Distributions: Analysis and Limitations, Soil Sci. Soc. Am. J. 56 (1992) 362–369. https://doi.org/10.2136/sssaj1992.03615995005600020005x.
[42] B. Yu, J. Li, Some fractal characters of porous media, Fractals. 9 (2001) 365–372. https://doi.org/10.1142/S0218348X01000804.
[43] C.G. Shull, The Determination of Pore Size Distribution from Gas Adsorption Data, J. Am. Chem. Soc. 70 (1948) 1405–1410. https://doi.org/10.1021/ja01184a034.
[44] E.P. Barrett, L.G. Joyner, P.P. Halenda, The Determination of Pore Volume and Area Distributions in Porous Substances. I. Computations from Nitrogen Isotherms, J. Am. Chem. Soc. 73 (1951) 373–380. https://doi.org/10.1021/ja01145a126.
[45] S. Sircar, Capillary condensation theory for adsorption of vapors on mesoporous solids, Surf. Sci. 164 (1985) 393–402. https://doi.org/10.1016/0039-6028(85)90754-X.
[46] J.M. De Burgh, S.J. Foster, H.R. Valipour, Prediction of water vapour sorption isotherms and microstructure of hardened Portland cement pastes, Cem. Concr. Res. 81 (2016) 134–150. https://doi.org/10.1016/j.cemconres.2015.11.009.
[47] S. Poyet, W. Dridi, V. L'Hostis, D. Meinel, Microstructure and diffusion coefficient of an old corrosion product layer and impact on steel rebar corrosion in carbonated concrete, Corros. Sci. 125 (2017) 48–58. https://doi.org/10.1016/j.corsci.2017.06.002.
[48] I. Langmuir, The Adsorption of Gases on Plane Surfaces of Glass, Mica and Platinum, J. Am. Chem. Soc. 40 (1918) 1361–1403. https://doi.org/doi: 10.1021/ja02242a004.
[49] J. Morgan, B.E. Warren, X-ray analysis of the structure of water, J. Chem. Phys. 6 (1938) 666–673. https://doi.org/10.1063/1.1750148.
[50] W.D. Harkins, G. Jura, Surface of Solids. X. Extension of the Attractive Energy of a Solid into an Adjacent Liquid or Film, the Decrease of Energy with Distance, and the Thickness of Films, J. Am. Chem. Soc. 66 (1944) 919–927. https://doi.org/10.1021/ja01234a024.
[51] J. Hagymassy, S. Brunauer, R.S. Mikhail, Pore structure analysis by water vapor adsorption I. t-curves for water vapor, J. Colloid Interface Sci. 29 (1969) 485–491. https://doi.org/10.1016/0021-9797(69)90132-5.
[52] S. Yamanaka, P.B. Malla, S. Komarneni, Water adsorption properties of alumina pillared clay, J. Colloid Interface Sci. 134 (1990) 51–58. https://doi.org/10.1016/0021-9797(90)90250-R.
[53] S.W. Wheatcraft, S.W. Tyler, An explanation of scale-dependent dispersivity in heterogeneous

aquifers using concepts of fractal geometry, Water Resour. Res. 24 (1988) 566–578.
[54] B. Yu, J. Li, Z. Li., M. Zou, Permeabilities of unsaturated fractal porous media, Int. J. Multiph. Flow. 29 (2003) 1625–1642. https://doi.org/10.1016/S0301-9322(03)00140-X.
[55] B. Yu, W. Liu, Fractal Analysis of Permeabilities for Porous Media, AIChE J. 50 (2004) 46–57. https://doi.org/10.1002/aic.10004.
[56] B. Yu, Analysis of Flow in Fractal Porous, Appl. Mech. Rev. 61 (2008) 050801. https://doi.org/10.1115/1.2955849.
[57] B. Yu, J. Cai, M. Zou, On the Physical Properties of Apparent Two-Phase Fractal Porous Media, Vadose Zo. J. 8 (2009) 177–186. https://doi.org/10.2136/vzj2008.0015.
[58] A.G. Hunt, M. Sahimi, Flow, Transport, and Reaction in Porous Media: Percolation Scaling, Critical-Path Analysis, and Effective Medium Approximation, Rev. Geophys. 55 (2017) 993–1078. https://doi.org/10.1002/2017RG000558.
[59] A.J. Katz, A.H. Thompson, Quantitative prediction of permeability in porous rock, Phys. Rev. B. 34 (1986) 8179–8181.
[60] A.J. Katz, A.H. Thompson, Prediction of rock electrical conductivity from mercury injection experiments, J. Geophys. Res. 92 (1987) 599–607.
[61] L. Guarracino, Estimation of saturated hydraulic conductivity Ks from the van Genuchten shape parameter α, Water Resour. Res. 43 (2007) 15–18. https://doi.org/10.1029/2006WR005766.
[62] S. Poyet, Determination of the intrinsic permeability to water of cementitious materials: Influence of the water retention curve, Cem. Concr. Compos. 35 (2013) 127–135. https://doi.org/10.1016/j.cemconcomp.2012.08.023.
[63] W. Chen, J. Liu, F. Brue, F. Skoczylas, C.A. Davy, X. Bourbon, J. Talandier, Water retention and gas relative permeability of two industrial concretes, Cem. Concr. Res. 42 (2012) 1001–1013. https://doi.org/10.1016/j.cemconres.2012.04.003.
[64] T.C. Powers, T.L. Brownyard, Studies of the Physical Properties of Hardened Portland Cement Paste, Bull. Portl. Cem. Assoc. 22 (1948) 356p.
[65] J. Hagymassy, I. Odler, M. Yudenfreund, J. Skalny, S. Brunauer, Pore structure analysis by water vapor adsorption. III. Analysis of hydrated calcium silicates and portland cements, J. Colloid Interface Sci. 38 (1972) 20–34. https://doi.org/10.1016/0021-9797(72)90215-9.
[66] Y.F. Houst, F.H. Wittmann, Influence of porosity and water content on the diffusivity of CO2 and O2 through hydrated cement paste, Cem. Concr. Res. 24 (1994) 1165–1176. https://doi.org/10.1016/0008-8846(94)90040-X.
[67] L.O. Nilsson, Long-term moisture transport in high performance concrete, Mater. Struct. 35 (2002) 641–649. https://doi.org/10.1007/BF02480357.
[68] V. Baroghel-Bouny, Water vapour sorption experiments on hardened cementitious materials Part I : Essential tool for analysis of hygral behaviour and its relation to pore structure, Cem. Concr. Res. 37 (2007) 414–437. https://doi.org/10.1016/j.cemconres.2006.11.019.
[69] A.G. Hunt, Comparing van Genuchten and percolation theoretical formulations of the hydraulic properties of unsaturated media, Vadose Zo. J. 3 (2004) 1483–1488.
[70] P.B. Bamforth, The relationship between permeability coefficients for concrete obtained using liquid and gas, Mag. Concr. Res. 39 (1987) 3–11.
[71] S. Tsivilis, E. Chaniotakis, G. Batis, C. Meletiou, V. Kasselouri, G. Kakali, A. Sakellariou, G. Pavlakis, C. Psimadas, The effect of clinker and limestone quality on the gas permeability, water absorption and pore structure of limestone cement concrete, Cem. Concr. Compos. 21 (1999) 139–146. https://doi.org/10.1016/S0958-9465(98)00037-7.
[72] M.I. Khan, C.J. Lynsdale, Strength, permeability, and carbonation of high-performance concrete, Cem. Concr. Res. 32 (2002) 123–131. https://doi.org/10.1016/S0008-8846(01)00641-X.
[73] H. Loosveldt, Z. Lafhaj, F. Skoczylas, Experimental study of gas and liquid permeability of a mortar, Cem. Concr. Res. 32 (2002) 1357–1363.
[74] I. Maruyama, Y. Nishioka, G. Igarashi, K. Matsui, Microstructural and bulk property changes in hardened cement paste during the first drying process, Cem. Concr. Res. 58 (2014) 20–34. https://doi.org/10.1016/j.cemconres.2014.01.007.
[75] I. Maruyama, N. Sakamoto, K. Matsui, G. Igarashi, Microstructural changes in white Portland cement paste under the first drying process evaluated by WAXS, SAXS, and USAXS, Cem. Concr. Res. 91 (2017) 24–32. https://doi.org/10.1016/j.cemconres.2016.10.002.
[76] G. Mesri, R.E. Olson, Mechanisms controlling the permeability of clays, Clays Clay Miner. 19 (1971) 151–158. https://doi.org/10.1346/CCMN.1971.0190303.
[77] M. Schramm, A.W. Warrick, W.H. Fuller, Permeability of soils to four organic liquids and water, Hazard. Waste Hazard. Mater. 3 (1986) 21–27. https://doi.org/10.1089/hwm.1986.3.21.

[78] F. Fernandez, R. Quigley, Viscosity and dielectric constant controls on the hydraulic conductivity of clayey soils permeated with water-soluble organics, Can. Geotech. J. 25 (1988) 582–589.
[79] A. Kaya, H.Y. Fang, Experimental evidence of reduction in attractive and repulsive forces between clay particles permeated with organic liquids, Can. Geotech. J. 42 (2005) 632–640. https://doi.org/10.1139/t04-099.
[80] S.L. Machado, L. da Silva Paes Cardoso, I.B. de Oliveira, D. de Faria Mariz, M. Karimpour-Fard, Modeling Soil Permeability When Percolated by Different Soil, Transp. Porous Media. 111 (2016) 763–793. https://doi.org/10.1007/s11242-016-0627-9.
[81] M. Auroy, S. Poyet, P. Le Bescop, J.M. Torrenti, T. Charpentier, M. Moskura, X. Bourbon, Impact of carbonation on unsaturated water transport properties of cement-based materials, Cem. Concr. Res. 74 (2015) 44–58. https://doi.org/10.1016/j.cemconres.2015.04.002.
[82] E. Garboczi, Permeability, diffusivity, and microstructural parameters: a critical review, Cem. Concr. Res. 20 (1990) 591–601.
[83] M.R. Nokken, R.D. Hooton, Using pore parameters to estimate permeability or conductivity of concrete, Mater. Struct. Constr. 41 (2008) 1–16. https://doi.org/10.1617/s11527-006-9212-y.
[84] V. Baroghel-Bouny, K. Kinomura, M. Thiery, S. Moscardelli, Easy assessment of durability indicators for service life prediction or quality control of concretes with high volumes of supplementary cementitious materials, Cem. Concr. Compos. 33 (2011) 832–847. https://doi.org/10.1016/j.cemconcomp.2011.04.007.
[85] A.S. El-Dieb, R.D. Hooton, Evaluation of the Katz-Thompson model for estimating the water permeability of cement-based materials from mercury intrusion porosimetry data, Cem. Concr. Res. 24 (1994) 443–455.
[86] B. Christensen, T. Mason, H. Jennings, Comparison of Measured and Calculated Permeabilities, Cem. Concr. Res. 26 (1996) 1325–1334.
[87] P. Tumidajski, B. Lin, On the validity of the Katz-Thompson equation for permeabilities in concrete, Cem. Concr. Res. 28 (1998) 643–647.
[88] P. Halamickova, R.J. Detwiler, Water permeability and chloride ion diffusion in Portland cement mortars: relationship to sand content and critical pore diameter, Cem. Concr. Res. 25 (1995) 790–802. https://doi.org/10.1016/0008-8846(95)00069-O.
[89] E. Drouet, S. Poyet, J.-M. Torrenti, Temperature influence on water transport in hardened cement pastes, Cem. Concr. Res. 76 (2015) 37–50. https://doi.org/10.1016/j.cemconres.2015.05.002.
[90] S. Poyet, B. Bary, E. Coppens, Analysis of water transport in unsaturated conditions: Comparison between labcrete and fieldcrete, Constr. Build. Mater. 205 (2019) 443–455. https://doi.org/10.1016/j.conbuildmat.2019.02.034.

606 **Nomenclature**

607 • R_m minimal pore radius (m)
608 • R_M maximal pore radius (m)
609 • D fractal dimension (without unit)
610 • N cumulated number of pores (without unit)
611 • r pore radius (m)
612 • n number of pores of radius r (without unit)
613 • $\emptyset$ porosity (without unit)
614 • S saturation ratio (without unit)
615 • S_a saturation ratio due to adsorption (without unit)
616 • S_c saturation ratio due to condensation (without unit)
617 • P liquid water pressure (Pa)
618 • t time (s)
619 • K intrinsic permeability (m^2)
620 • k_r relative permeability to water (without unit)
621 • η dynamic water viscosity (Pa s)
622 • m constant of van Genuchten equation (without unit)
623 • P_0 constant of van Genuchten equation (Pa)
624 • t_w thickness of the water layer adsorbed on the pore walls (m)
625 • t_m thickness of the water monolayer (m)
626 • k constant of Langmuir model (without unit)
627 • h relative humidity (without unit)
628 • r_K Kelvin radius (m)
629 • M water molar mass (kg/mol)
630 • σ water surface tension (N/m)
631 • ρ water density (kg/m^3)
632 • R universal gas constant (J/mol/K)
633 • T absolute temperature (K)
634 • q flowrate through a pore of radius r (m^3/s)
635 • Q_t flowrate through all the pores (m^3/s)
636 • ΔP pressure difference applied to the pores (Pa)
637 • F formation factor (without unit)
638 • d_c critical pore diameter (m)

639